

Synthesis, crystal structure, spectroscopic, and photoreactive properties of a ruthenium(II)-mononitrosyl complex



Marine Tassé, Hasan S. Mohammed, Chloé Sabourdy, Sonia Mallet-Ladeira, Pascal G. Lacroix*, Isabelle Malfant*

Laboratoire de Chimie de Coordination du CNRS, UPR 8241, 205 route de Narbonne, F-31077 Toulouse, France

ARTICLE INFO

Article history:

Received 16 June 2016

Accepted 4 September 2016

Available online 15 September 2016

Keywords:

Ruthenium complexes

Nitric oxide

Molecular switch

NO release

Computational chemistry

ABSTRACT

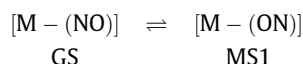
A compound of formula $[\text{Ru}^{\text{II}}\text{Cl}(\text{NO})(\text{Cl-py})_4](\text{PF}_6)_2$, in which Cl-py is the 4-chloropyridine, has been synthesized in four steps and fully characterized. It crystallizes in the $P\bar{1}$ triclinic space group as $[\text{Ru}^{\text{II}}\text{Cl}(\text{NO})(\text{Cl-py})_4](\text{PF}_6)_2 \cdot 1.25\text{H}_2\text{O}$. Upon irradiation at $\lambda = 473$ nm in the solid state, the N-bounded nitrosyl ligand (ground state GS: $[\text{Ru}^{\text{II}}(\text{NO})]$) turns into O-bounded nitrosyl metastable state 1 (MS1: $[\text{Ru}^{\text{II}}(\text{ON})]$). The population of the long-lived metastable $\text{Ru}^{\text{II}}(\text{ON})$ isomer is equal to 27% on powder samples, therefore 3 times less than that of the parent $[\text{Ru}^{\text{II}}\text{Cl}(\text{NO})(\text{py})_4](\text{PF}_6)_2$ derivative. Spectroscopy and TD-DFT studies are proposed to find a rational for this difference at the molecular level, which is tentatively related to different UV–visible spectra in the metastable $\text{Ru}^{\text{II}}(\text{ON})$ isomer. Surprisingly, and while the switching efficiency of $[\text{Ru}^{\text{II}}\text{Cl}(\text{NO})(\text{Cl-py})_4](\text{PF}_6)_2$ appears relatively modest, its capability for releasing the biologically active nitric oxide (NO^\cdot) radical under irradiation in solution is found to be about 100 times that of the $[\text{Ru}^{\text{II}}\text{Cl}(\text{NO})(\text{py})_4](\text{PF}_6)_2$ derivative.

© 2016 Elsevier Ltd. All rights reserved.

1. Introduction

Photochromism, in which a molecule is reversibly photo-transformed between two isomers having different absorption spectra, has been a promising research topic in modern molecular science [1], in relation to the intriguing concepts of molecular switches and memories [2], and molecular machines [3]. Various classes of molecules have been reported to possess photo-switching capabilities, such as diarylethenes [4], spiropyrans [5], or azobenzenes [6]. A particular interest is devoted to solid state photo-isomerization which could lead to applications for data storage, and ultrafast photonic devices [7–10]. Although it may occasionally be observed in few classes of photochromic species like spiropyrans [11,12], it is usually hampered by the effect of the crystal rigidity which prevents any significant intramolecular motion involved in the isomerization process. Therefore, solid state isomerization is mainly observed in systems in which the atomic rearrangements are restricted to the minimum. This requirement is fulfilled in N-salicylidene anilines derivatives which undergo a tautomeric (proton transfer supported by the solid state environment) equilibrium between ketonic and enolic forms, if we [13,14], with typical

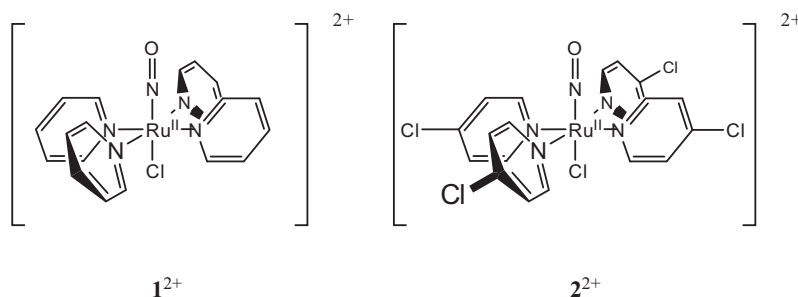
population of metastable states limited to a few percent [15], and in metal-(nitrosyl) complexes (N-bounded nitrosyl, ground state GS), which are reversibly isomerized to a metal-(*iso*-nitrosyl) (O-bounded nitrosyl, metastable state MS1), as follows:



Indeed, since the discovery of long-lived metastable states in sodium nitroprusside ($\text{Na}_2[\text{Fe}(\text{CN})_5(\text{NO})] \cdot 2\text{H}_2\text{O}$) [16], the NO/ON isomerization has been observed in various metal-nitrosyl derivatives (e.g. iron, ruthenium, osmium, manganese, iron, nickel and platinum) in solid state [17–21]. Few years ago, we have observed a remarkably large population ($\geq 92\%$) of the metastable state MS1, in $[\text{Ru}^{\text{II}}\text{Cl}(\text{NO})(\text{py})_4]^{2+}$ (1^{2+} , in Scheme 1) after irradiation of a crystal of $[\text{Ru}^{\text{II}}\text{Cl}(\text{NO})(\text{py})_4](\text{PF}_6)_2 \cdot 0.5\text{H}_2\text{O}$ at $\lambda = 473$ nm [22], while the previous highest populations reported was that of Hauser, in 1977, with only 50% of MS1 in a single crystal of sodium nitroprusside [16]. In a previous investigation [23], we have targeted the role devoted to the solid state environment to account for this effect. Indeed, we have observed that the population of the metastable $[\text{Ru}^{\text{II}}\text{Cl}(\text{ON})(\text{py})_4]^{2+}$ units strongly depends on the nature of the counterions, present in the vicinity of the nitrosyl ligand. In this second investigation, we wish to target the influence of the intramolecular electronic properties to the rate of isomerization. $[\text{Ru}^{\text{II}}\text{Cl}(\text{NO})(\text{Cl-py})_4](\text{PF}_6)_2$, an alternative system closely related to

* Corresponding author. Fax: +33 5 61 55 30 03.

E-mail addresses: pascal.lacroix@lcc-toulouse.fr (P.G. Lacroix), isabelle.malfant@lcc-toulouse.fr (I. Malfant).



Scheme 1. Ruthenium(II)-nitrosyl based cations.

$[\text{Ru}^{\text{II}}\text{Cl}(\text{NO})(\text{py})_4](\text{PF}_6)_2$ will be described and fully characterized. Then, the solid-state photochromic properties of both $[\text{Ru}^{\text{II}}\text{Cl}(\text{NO})(\text{Cl-py})_4](\text{PF}_6)_2$, and $[\text{Ru}^{\text{II}}\text{Cl}(\text{NO})(\text{py})_4](\text{PF}_6)_2$ will be compared. The observed differences will be tentatively rationalized from a computational investigation of the spectroscopic properties of the switchable cations conducted within the framework of the time-dependent density functional theory (TD-DFT) method [24]. The molecular structure of the two cations involved in this study is shown in Scheme 1 (2^{2+} for $[\text{Ru}^{\text{II}}\text{Cl}(\text{NO})(\text{Cl-py})_4]^{2+}$).

2. Experimental

2.1. General procedures

$[\text{Ru}^{\text{II}}\text{Cl}(\text{NO})(\text{py})_4](\text{PF}_6)_2$ was synthesized following the previously reported procedure [22]. 4-Chloropyridine hydrochloric, 4-aminopyridine and the Griess reagent used for the NO detection were obtained from Sigma. Ruthenium trichloride hydrate $\text{Ru}^{\text{III}}\text{Cl}_3 \cdot x\text{H}_2\text{O}$ was obtained from Strem Chemicals. The solvents were analytical grade and used without further purification. Elemental analyses were performed at LCC with a Perkin Elmer 2400 serie II Instrument. ^1H NMR spectra were obtained at 298 K in D_2O , or $(\text{CD}_3)_2\text{SO}$ as internal reference and were recorded on a Bruker Avance 400. Chemical shifts (δ) are reported in ppm and coupling constants (J) in Hz. Infrared spectra were recorded on a Perkin Elmer Spectrum 100 FT-IR Spectrometer, using a diamond ATR. Ultraviolet–visible spectra were recorded on Jasco V-670 spectrophotometer.

2.2. Synthesis of $[\text{Ru}^{\text{II}}\text{Cl}(\text{NO})(\text{Cl-py})_4](\text{PF}_6)_2$

“Ruthenium (II) blue” solution. $\text{RuCl}_3 \cdot x\text{H}_2\text{O}$ (500 mg, 2.4 mmol) was dissolved in 25 mL of hydrochloric acid (3 mol L^{-1}) and stirred for 20 min. The solution was then heated to 100°C under vacuum until dryness (black product). The dry RuCl_3 residue was dissolved in a mixture of ethanol (30 mL) and distilled water (25 mL) and was heated to 100°C for 4 h to give “Ruthenium (II) blue” (intermediate). CAUTION: the solution of “ruthenium blue” is unstable and has to be readily used for the synthesis of the desired complexes.

$[\text{Ru}^{\text{II}}\text{Cl}_2(4\text{-NH}_2\text{py})_4]$. 4-Aminopyridine (1.534 g, 16.32 mmol) was dissolved in 15 mL (1/3 H_2O –2/3 ethanol) and was added to “Ruthenium (II) blue” (500 mg, 2.4 mmol $\text{RuCl}_3 \cdot x\text{H}_2\text{O}$). The solution was refluxed for 1.5 h, and then concentrated to the half of its initial volume. 50 mL of acetone was added to precipitate the complex. Yield (325 mg, 25%), black powder. Elemental analysis found: C, 43.89; H, 4.48; N, 20.50%. $\text{C}_{20}\text{H}_{24}\text{Cl}_2\text{N}_8\text{Ru}$ requires C, 43.80; H, 4.41; N, 20.43%. ^1H NMR, (D_2O , 400 MHz, 298 K): δ 7.90 (8H α , d, J 7.17), 6.76 (8H β , d, J 7.12). IR (KBr) ν_{max} (cm^{-1}): 3304 (NH_2), 3180 (NH_2), 1611 (NH_2), 1508 ($\text{C}=\text{N}$).

$[\text{Ru}^{\text{II}}\text{Cl}(\text{NO})(\text{Cl-py})_4](\text{PF}_6)_2$. $[\text{Ru}^{\text{II}}\text{Cl}_2(4\text{-NH}_2\text{py})_4]$ (271 mg, 0.494 mmol) was dissolved in a mixture of 20 mL of ethanol and 5 mL of distilled water. Sodium nitrite (204 mg, 2.96 mmol) in solution in water (5 mL) was added to the complex. The resulting solution was refluxed for 4 h. 4 mL of hydrochloric acid (37%) was then added and the solution was refluxed for additional 45 min. The solution was left to cool down to room temperature, then NH_4PF_6 (260 mg, 1.6 mmol in 3 mL of water) was added to precipitate the complex as an orange powder. The solution was filtered, washed with water and dried under vacuum. Yield (204 mg, 45%). Elemental analysis found: C, 25.95; H, 1.78; N, 8.01%. $\text{C}_{20}\text{H}_{16}\text{Cl}_5\text{F}_{12}\text{N}_5\text{OP}_2\text{Ru}$ requires C, 26.38; H, 1.77; N, 7.69%. ^1H NMR($(\text{CD}_3)_2\text{SO}$, 300 MHz, 298 K): δ 8.54 (8H α , d, 3J 5.2), 7.92 (8H β , d, 3J 5.4). IR (KBr) ν_{max} cm^{-1} : 3044 ($\text{C-H}_{\text{aromatic}}$), 1910 (N-O), 1614 ($\text{C}=\text{N}$), 1424 ($\text{C}=\text{C}$), 825 (P-F).

2.3. X-ray crystallography

Single crystals suitable for X-ray diffraction were obtained as yellow plates by slow evaporation of a solution of $[\text{Ru}^{\text{II}}\text{Cl}(\text{NO})(\text{Cl-py})_4](\text{PF}_6)_2$ in an acetonitrile/water mixture. Data were collected at low temperature (100(2) K) on a Bruker Kappa Apex II diffractometer equipped with a 30 W air-cooled microfocus, using $\text{MoK}\alpha$ radiation ($\lambda = 0.71073 \text{ \AA}$), and an Oxford Cryosystems Cryostream cooler device. Phi- and omega- scans were used for data collection. The structure was solved by direct methods with SHELXS-97 [25]. All non-hydrogen atoms were refined anisotropically by means of least-squares procedures on F2 with the aid of the program SHELXL-97 [25]. All the hydrogen atoms were refined isotropically at calculated positions using a riding model except those of water molecules which were not found in difference Fourier maps and therefore they were not included into the model. The oxygen atom of one water molecule is disordered over two positions (O2 and O2') in a 43:57 ratio and the water molecule O3 has an occupancy of 0.25. In the solvent region some residual electron density were difficult to model, therefore the SQUEEZE function of PLATON [26] was used to eliminate the contribution of this electron density from the intensity data for the final refinement. The crystal structure of $[\text{Ru}^{\text{II}}\text{Cl}(\text{NO})(\text{Cl-py})_4](\text{PF}_6)_2$ has been deposited with the Cambridge Crystallographic Data Center.

2.4. Computational methods

The molecular geometries of 1^{2+} and 2^{2+} were computed using the GAUSSIAN-09 program package [27] within the framework of the DFT at the B3LYP/6-31G* level [28–30], the LANL2DZ pseudopotential being used to account for relativistic effects on the ruthenium atom [31]. The widely applied B3LYP functional was selected for a better consistency with our previous investigation of 1^{2+} [23]. The computations were performed in the presence of acetonitrile with the SCRf method implemented in Gaussian, using the

polarizable continuum model (PCM) [32]. Vibrational analysis was performed at the same level in order to establish the presence of a minimum on the potential energy surfaces. In a first step of computation, no symmetry was imposed. However, the C_4 symmetry was observed in the final geometries within a tolerance of 0.002 Å for both cations. Therefore, the actual geometries were assumed to be C_4 in the final computations.

In a second step, the UV–visible spectra were computed at the PBE0/6-31G* level. The choice for this functional was motivated by the fact that it reproduced fairly well the experimental spectra by comparison with B3LYP, TPSSh, and B3PW91, previously used in the investigation of ruthenium(II) complexes with polypyridines and chlorides ligands [23,33,34] (Supplementary Materials: Fig. S1).

2.5. Photochemistry

Photoswitch in the solid state. IR spectra were recorded on a Perkin Elmer GX2000 spectrophotometer. $[\text{Ru}^{\text{II}}\text{Cl}(\text{NO})(\text{Cl-py})_4](\text{PF}_6)_2$ (1 mg) was mixed with KBr (99 mg), grinded and pressed to a pellet (1 ton, 2 min). The sample was cooled down to 100 K, in a SPECAC (P/N 20600) cryostat, and irradiated during 180 min with monochromatic light (diode laser: $\lambda = 473$ nm). The experiment was performed in the same pelletizing and temperature conditions on $[\text{Ru}^{\text{II}}\text{Cl}(\text{NO})(\text{py})_4](\text{PF}_6)_2$ to ensure a reliable comparison.

NO release. The UV–visible spectra were recorded on 2 mL of non-deoxygenated solutions of the nitrosyl complexes (0.93 mmol/L) in acetonitrile, under irradiation realized with a Muller reactor device equipped with a cooling water filter and a mercury arc lamp equipped with appropriate interference filter to isolate the desired irradiation wavelength ($\lambda_{\text{max}} = 436$ nm, intensity 9 mW). The sample solutions were placed in a quartz cuvette of 1 cm pathlength, and stirred continuously. The temperature was maintained at 27 °C during the whole experiment. Details on kinetic studies with the use of the Griess reagent are reported in Supplementary Materials.

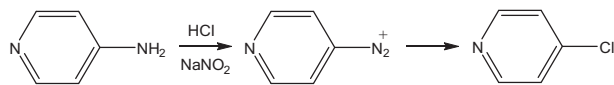
3. Results and discussion

3.1. Synthesis and characterization of $[\text{Ru}^{\text{II}}\text{Cl}(\text{NO})(\text{Cl-py})_4](\text{PF}_6)_2$

Following the general route previously described for $[\text{Ru}^{\text{II}}\text{Cl}(\text{NO})(\text{py})_4](\text{PF}_6)_2$ [22], $[\text{Ru}^{\text{II}}\text{Cl}(\text{NO})(\text{Cl-py})_4](\text{PF}_6)_2$ was synthesized from $\text{Ru}^{\text{III}}\text{Cl}_3$ and 4-chloropyridine by a four-steps procedure with slight variations. While $[\text{Ru}^{\text{II}}\text{Cl}(\text{NO})(\text{py})_4](\text{PF}_6)_2$ was obtained in pyridine acting both as ligand and solvent, $[\text{Ru}^{\text{II}}\text{Cl}(\text{NO})(\text{Cl-py})_4](\text{PF}_6)_2$ was synthesized in ethanol in which 4-chloropyridine (Cl-py) was dissolved. However, this route implies a tedious purification process, which brings down the overall yield. By contrast, $[\text{Ru}^{\text{II}}\text{Cl}(\text{NO})(\text{Cl-py})_4](\text{PF}_6)_2$ was also unexpectedly obtained from the 4-aminopyridine with a better yield (see Section 2). $[\text{Ru}(\text{4-NH}_2\text{py})_4\text{Cl}_2]$ in presence of an excess of sodium nitrite and hydrochloric acid leads to the diazonium salt that finally forms the 4-chloropyridine as described in Scheme 2.

3.2. Crystal structure description

$[\text{Ru}^{\text{II}}\text{Cl}(\text{NO})(\text{Cl-py})_4](\text{PF}_6)_2$ crystallizes in the $P\bar{1}$ triclinic space group. The asymmetric unit cell, shown in Fig. 1, is built up from



Scheme 2. Synthetic route towards 4-chloropyridine.

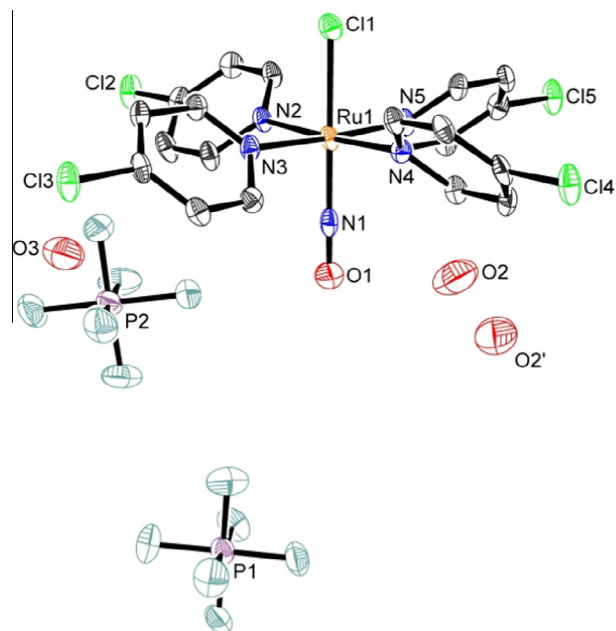


Fig. 1. Asymmetric unit for $[\text{Ru}^{\text{II}}\text{Cl}(\text{NO})(\text{Cl-py})_4](\text{PF}_6)_2 \cdot 1.25\text{H}_2\text{O}$. Displacement ellipsoids are drawn at the 50% probability level. Hydrogen atoms are omitted for clarity.

one $[\text{Ru}^{\text{II}}\text{Cl}(\text{NO})(\text{Cl-py})_4](\text{PF}_6)_2$ entity and molecules of water. One molecule of water is disordered between two sites, with occupation rate of 0.43 and 0.57, for O(2) and O(2'), respectively. A second molecule labeled as O(3) is present without disorder, with an occupation rate of 0.25. Each $[\text{Ru}^{\text{II}}\text{Cl}(\text{NO})(\text{Cl-py})_4]^{2+}$ unit is linked to four neighboring cationic species through short contacts observed between the chlorine atoms of adjacent complexes (Cl...Cl distance around 2.25 Å) as illustrated in Fig. 2, so the overall packing

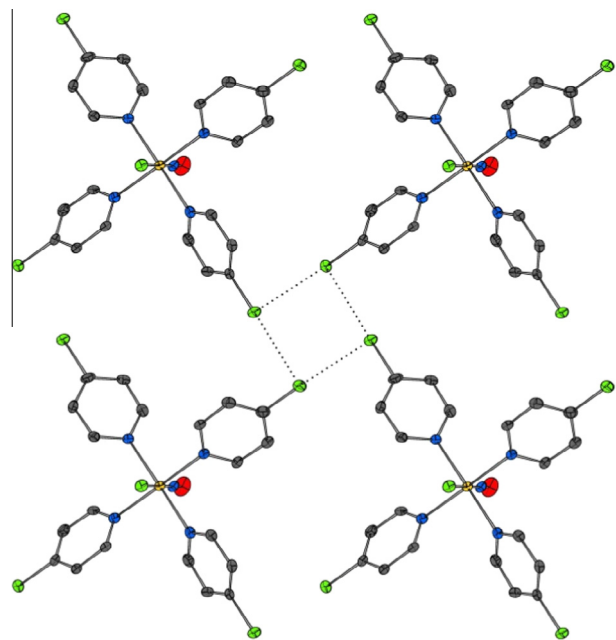


Fig. 2. Cl–Cl Van der Waals contacts shown by dashed lines, between adjacent $[\text{Ru}^{\text{II}}\text{Cl}(\text{NO})(\text{Cl-py})_4]^{2+}$ cations. Displacement ellipsoids are drawn at the 50% probability level. Hydrogen atoms, water molecules and counter-anions are omitted for clarity.

results from slabs of cations, with PF_6^- anions and water molecules inserted in between (Fig. 3).

The main bond lengths and angles in the coordination sphere of the 2^{2+} cation are gathered in Table 2 and compared with those of 1^{2+} , previously reported [22](a). In the solid state, the symmetry of 2^{2+} is C_4 , within a tolerance of 0.2 Å. At first glance, the C_4 symmetry can be assumed for the solid state geometry of 1^{2+} as well, but within a tolerance enlarged to 0.6 Å and 0.8 Å, for the two cations present in the asymmetric unit cell, 1^{2+} (A) and 1^{2+} (B), respectively. The first thing to check on the molecular structure is the conformation of the Ru–NO linkage. With a Ru–N–O angle of $179.6(4)^\circ$ supported by an experimental ν_{NO} vibrational mode at 1910 cm^{-1} , the electron configuration in the $\{\text{Ru–NO}\}^6$ corresponds to $\text{Ru}^{\text{II}}(\text{NO})^+$. Indeed, it has clearly been established that, for mononitrosyl $\{\text{M–NO}\}^6$ photochromic complexes such as $[\text{Fe}^{\text{II}}(\text{CN})_5(\text{NO})]^{2-}$ or $[\text{Ru}^{\text{II}}\text{Cl}(\text{NO})(\text{py})_4]^{2+}$, the M–NO group is linear in the ground state and the ν_{NO} vibrational mode is ranging in the 1900 cm^{-1} region [35].

The data gathered in Table 2, suggest that the introduction of chloro substituents, while located at the periphery of the molecule, may introduce significant changes in the internal conformations around the metal atom. The largest difference observed in the first coordination spheres of Ru^{II} for 1^{2+} and 2^{2+} is 0.03 Å at the Ru–Cl bond length, which corresponds to a decrease of 1.25% of the value on passing from 1^{2+} to 2^{2+} . The other averaged metal distances differences fall in the range of esds uncertainty. Something interesting to point out is the surprisingly short NO bond length of 1.125(5) Å observed in 2^{2+} , which corresponds to a shortening of 1.87% of the averaged value found in 1^{2+} (1.146(2) Å and 1.147(2) Å, for (A) and (B), respectively). Nevertheless, this value is in the range of magnitude of 1.117(4)–1.126(5) Å found in related $[\text{Ru}^{\text{II}}\text{Cl}(\text{NO})(\text{py})_4]^{2+}$ based crystal structures, and is therefore fully acceptable [23].

In order to understand if these differences arise from intramolecular electronic effects rather than from crystal packing effects, the DFT computed conformations are provided in Table 2. The data clearly indicate that both 1^{2+} and 2^{2+} cations exhibit grossly the same molecular geometries. Concerning the first coordination sphere, the computation confirms that the largest difference is expected in the Ru–Cl bond length, but it is reduced from 0.029 Å (X-ray) to 0.006 Å (DFT). Similarly, the shortening of the NO bond length is modest in the computed 2^{2+} species (0.002 Å)

Table 1

Crystal data and structure refinement parameters for $[\text{RuCl}(\text{NO})(\text{Cl–py})_4](\text{PF}_6)_2 \cdot 1.25(\text{H}_2\text{O})$.

Chemical formula	$\text{C}_{20}\text{H}_{16}\text{Cl}_5\text{N}_5\text{ORu}, 2(\text{F}_6\text{P}), 1.25(\text{H}_2\text{O})$
Formula weight	933.14
Crystal system	triclinic
Space group	$P\bar{1}$
T (K)	100(2)
Wavelength (Mo K α) (Å)	0.71073
a (Å)	11.846(2)
b (Å)	11.9150(18)
c (Å)	12.379(2)
α ($^\circ$)	89.918(5)
β ($^\circ$)	73.153(5)
γ ($^\circ$)	89.858(5)
V (Å 3)	1672.2(5)
Z	2
D_{calc} (g cm $^{-3}$)	1.848
Absorption coefficient (mm $^{-1}$)	1.062
Reflections collected	23,990
Uniques	6082
R_{int}	0.0588
R_1^a	0.0742
wR_2^b [$I > 2\sigma(I)$]	0.1080
Goodness-of-fit (GOF) on F^2	1.003

$$^a R_1 = \frac{\sum |F_o| - |F_c|}{\sum |F_o|}$$

$$^b wR_2 = \left[\frac{\sum w(F_o^2 - F_c^2)^2}{\sum (wF_o^2)^2} \right]^{1/2}$$

compared to the X-ray data. These experimental differences may tentatively be related to different solid state environments around the cations. Indeed, few short contacts involving the NO ligands are evidenced as follows: in 1^{2+} (A), two short O–F distances of 2.908(2) Å and 2.912(2) Å are present between NO and different PF_6^- anions; in 1^{2+} (B), one O–F distance of 2.932(2) Å is present between NO and a first PF_6^- anion, two O–F distances of 2.801(2) Å and 2.898(2) Å are present between NO and a second PF_6^- anion, and one O–H distance of 2.616(2) Å is present between NO and an hydrogen atom of a pyridine of a neighboring cation; in 2^{2+} , one O–F distance of 2.952(5) Å is present between NO and a PF_6^- anion, and one O–O distance of 2.930 Å is present between NO and a molecule of water. To summarize, two short contacts are observed involving the NO ligand of 1^{2+} (A), and 2^{2+} , and four short contacts are observed in the case of 1^{2+} (B).

In the next section, spectroscopic investigations are reported to further characterize the effect of the chloro substituents on the

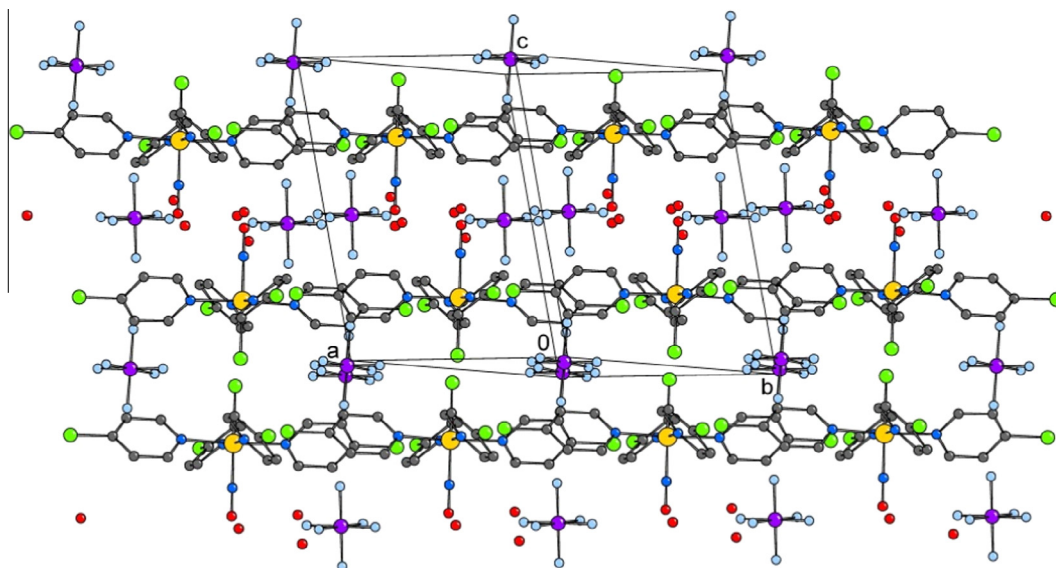


Fig. 3. Crystal packing for $[\text{Ru}^{\text{II}}\text{Cl}(\text{NO})(\text{Cl–py})_4](\text{PF}_6)_2 \cdot 1.25\text{ H}_2\text{O}$ projected in the (110) plane, showing the cationic slabs, maintained by Cl...Cl short contacts.

Table 2
Comparison of crystallographic and computed bond lengths (in Å) and angles (in °) for 1^{2+} , and 2^{2+} .

	X-ray		2^{2+}	DFT	
	1^{2+}			$1^{2+}(C_4)$	$2^{2+}(C_4)$
	Molecule A ¹	Molecule B ¹			
Ru(1)–N(1) _{NO}	1.7550(17)	1.7537(16)	1.767(4)	1.771	1.775
Ru(1)–N(2) _{py}	2.1044(17)	2.1036(16)	2.103(4)	2.150	2.148
Ru(1)–N(3) _{py}	2.1041(17)	2.1015(17)	2.100(4)	2.150	2.148
Ru(1)–N(4) _{py}	2.1069(18)	2.1050(17)	2.098(3)	2.150	2.148
Ru(1)–N(5) _{py}	2.1142(17)	2.1213(16)	2.114(4)	2.150	2.148
Ru(1)–Cl(1)	2.3206(6)	2.3231(5)	2.2927(13)	2.367	2.361
N(1)–O(1)	1.146(2)	1.147(2)	1.125(5)	1.143	1.141
Cl(1)–Ru(1)–N _{py} ²	88.4	88.0	88.2	88.0	88.0
N(1) _{NO} –Ru(1)–N _{py} ²	91.6	92.1	91.8	92.0	92.0
Ru(1)–N(1)–O(1)	178.30(16)	172.42(16)	179.6(4)	180.0	180.0

¹ Reference [22a].

² Averaged value.

electronic properties and switching capabilities, at the molecular level.

3.3. Spectroscopic properties

The experimental UV–visible spectra of $[\text{Ru}^{\text{II}}\text{Cl}(\text{NO})(\text{Cl-py})_4](\text{PF}_6)_2$ ($2(\text{PF}_6)_2$) and $[\text{Ru}^{\text{II}}\text{Cl}(\text{NO})(\text{py})_4](\text{PF}_6)_2$ ($1(\text{PF}_6)_2$) are shown in Fig. 4. In both cases, the overall spectra exhibit the same qualitative shape, with a low lying band having absorption maxima located at 457 nm ($\epsilon = 665 \text{ mol}^{-1} \text{ L cm}^{-1}$) and 448 nm ($\epsilon = 151 \text{ mol}^{-1} \text{ L cm}^{-1}$), for $2(\text{PF}_6)_2$, and $1(\text{PF}_6)_2$, respectively, and very intense bands below 300 nm. What immediately strikes in the observation of the figure is the large difference in the intensity of the spectra, for so closely related species. Indeed, the absorbance appears at least 4 times more intense in $2(\text{PF}_6)_2$ than in $1(\text{PF}_6)_2$. The theoretical spectra were therefore computed to try to rationalize these differences (Fig. S1). The results are gathered in Table 3. Experiment and computation indicate a tendency for red shift and higher intensity in 2^{2+} , although the full extent of the enhancement of the extinction coefficient ($\epsilon_{2^{2+}} \approx 4 \times \epsilon_{1^{2+}}$) is not fully explained by the computation ($f_{2^{2+}} \approx 2 \times f_{1^{2+}}$). At the orbital level, the low-lying bands arise from two transitions degenerated for symmetry reason in the C_4 point group. They involve contributions of the HOMO – 3 \rightarrow LUMO and LUMO + 1, and the HOMO \rightarrow LUMO and LUMO + 1 excitations, for 1^{2+} and 2^{2+} , respectively, in which an important charge transfer towards the nitrosyl ligand is observed in any cases. The involved orbitals are shown in Fig. 5. Except for a weak contribution of a p orbital of the chlorine atoms at the HOMO level of 2^{2+} , the electronic properties appear closely related in both species. In particular, the strong antibonding character observed between the

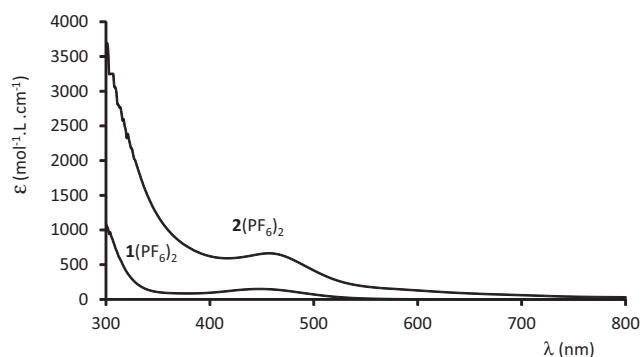


Fig. 4. Experimental UV–visible spectra of $[\text{Ru}^{\text{II}}(\text{Cl-py})_4\text{ClNO}](\text{PF}_6)_2$ ($2(\text{PF}_6)_2$) compared to that of the parent $[\text{Ru}^{\text{II}}(\text{py})_4\text{ClNO}](\text{PF}_6)_2$ ($1(\text{PF}_6)_2$), in acetonitrile.

ruthenium atom and the nitrogen of the nitrosyl ligand at the LUMO and LUMO + 1 level in both cases supports the resulting photo-lability of the NO fragment.

3.4. Photochromic properties

We have previously reported a remarkably large population ($\geq 92\%$) of metastable state in $[\text{Ru}^{\text{II}}\text{Cl}(\text{NO})(\text{py})_4](\text{PF}_6)_2$ [22]. In this first report, the measurements were carried out on small-sized single crystals. By contrast, the present investigation is based on powdered samples diluted in diffusing KBr pellets. Infrared spectroscopy upon irradiation at 100 K on ruthenium nitrosyl can evidence the reversible structural change associated with the formation of metastable state MS1 from the ground state GS (Fig. 6). GS/GM1 conversion is easily observable by the shift of ν_{NO} vibration frequency to lower frequencies. In $[\text{Ru}^{\text{II}}\text{Cl}(\text{NO})(\text{Cl-py})_4](\text{PF}_6)_2$, the ν_{NO} frequency is observed at 1910 cm^{-1} for GS and a band occurs at 1762 cm^{-1} for MS1. The peak area ratio before and after irradiation at 1910 cm^{-1} , in the absorbance spectra allows evaluating the population of the metastable state MS1. In previous work [22,23] on powder sample of $[\text{Ru}^{\text{II}}\text{Cl}(\text{NO})(\text{py})_4](\text{PF}_6)_2$, the population was found to be 76%. In $[\text{Ru}^{\text{II}}\text{Cl}(\text{NO})(\text{Cl-py})_4](\text{PF}_6)_2$, this ratio was decreasing down to 27%.

A time of irradiation of 180 min led to no more apparent evolution of the $\nu_{(\text{NO})}$ IR spectra, however the completeness of the switch may not have been strictly achieved, according to previous observations which indicate that the population of metastable state may be surpassed in single crystal experiments [36]. Indeed, the yield of photoconversion of $[\text{Ru}^{\text{II}}\text{Cl}(\text{NO})(\text{py})_4]^{2+}$ to $[\text{Ru}^{\text{II}}\text{Cl}(\text{ON})(\text{py})_4]^{2+}$ is reduced from 92% to 76%. Interestingly, and under the same experimental conditions, the population of metastable state of $[\text{Ru}^{\text{II}}\text{Cl}(\text{NO})(4\text{Cl-py})_4](\text{PF}_6)_2$, is only 27%, about three times less than that of the parent $[\text{Ru}^{\text{II}}\text{Cl}(\text{NO})(\text{py})_4](\text{PF}_6)_2$.

In the previous sections, we have pointed out that the solid state environments and the presence of chloro substituents could modulate the overall electronic responses of 1^{2+} , and 2^{2+} , although it is difficult to estimate the real magnitude of both effects, precisely. In an attempt to get more insights at the intramolecular level on the comparison of the switching capabilities, the Gibbs free energies have been computed for the following equilibria:

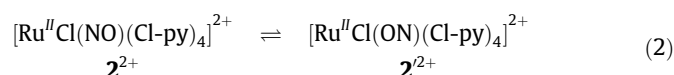
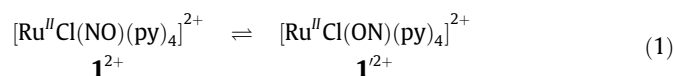


Table 3

Comparison of experimental and TD-DFT data for 1^{2+} and 2^{2+} : absorption maxima (λ_{\max} in nm), extinction coefficients (ϵ in $\text{mol}^{-1} \text{L cm}^{-1}$), oscillator strengths (f), main component and character of the configuration interaction (CI) expansion.

Compound	UV-vis spectra		TD-DFT computations		Dominant composition of the CI expansion ¹	Character	
	λ_{\max}	ϵ	Transition	λ_{\max}			f
1^{2+}	448	150	1 → 3	419	0.0020	$0.672 \chi_{104 \rightarrow 108}$ $-0.672 \chi_{104 \rightarrow 109}$	$d_{xy} \rightarrow d_{xz}-\pi_x(\text{NO})^*$ $d_{xy} \rightarrow d_{yz}-\pi_y(\text{NO})^*$
			1 → 4	419	0.0020		
2^{2+}	457	665	1 → 2	429	0.0041	$0.537 \chi_{139 \rightarrow 141} + 0.321 \chi_{139 \rightarrow 140}$ $0.537 \chi_{139 \rightarrow 140} - 0.321 \chi_{139 \rightarrow 141}$	$d_{xy} + 4e(\text{pCl}) \rightarrow d_{xz}-x(\text{NO})^*$ $d_{xy} + 4e(\text{pCl}) \rightarrow d_{yz}-\pi_y(\text{NO})^*$
			1 → 3	429	0.0041		

Orbitals 139, 140, and 141 are the HOMO, LUMO, and LUMO + 1, respectively, for 2^{2+} .

¹ Orbitals 104, 108, and 109 are the HOMO – 3, LUMO, and LUMO + 1, respectively, for 1^{2+} .

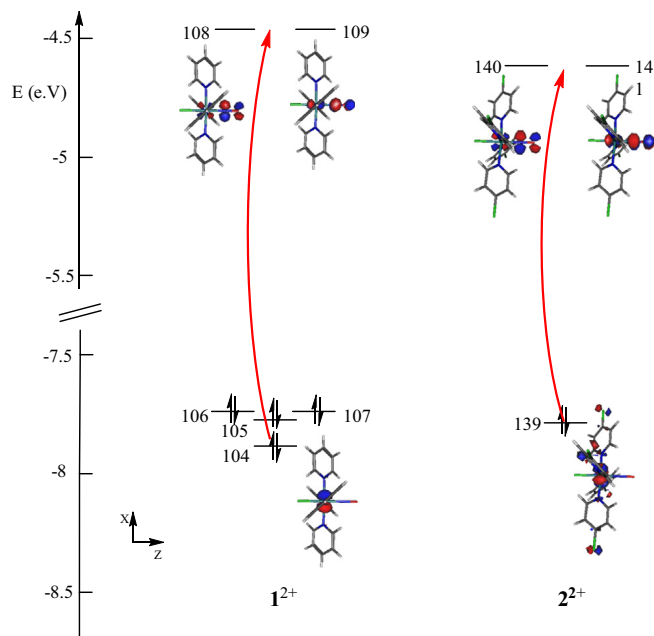


Fig. 5. Dominant orbitals involved in the low-lying transitions of 1^{2+} and 2^{2+} .

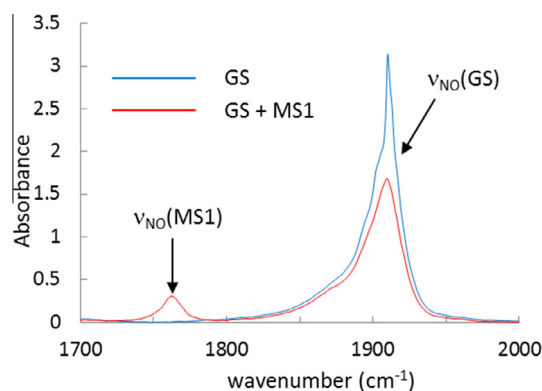


Fig. 6. Infrared spectra of $2(\text{PF}_6)_2$ without irradiation (blue) and after irradiation (red). (Color online.)

The results lead to $\Delta G^\circ = 38.1 \text{ kcal mol}^{-1}$ and $37.8 \text{ kcal mol}^{-1}$, for Eqs. (1) and (2), respectively. Therefore, there is no thermodynamic reason to infer that the process described in (1) should far be more efficient than that in (2).

A second approach implies the analysis of the effect of the light on the metastable state. Indeed, the irradiation has to be conducted at a wavelength in which the metastable state does not absorb in order to avoid a possible back isomerization and hence a poorly efficient isomerization process. The optical properties of both

ruthenium-iso-nitrosyl $[\text{Ru}^{\text{II}}(\text{ON})]$ (1^{2+} and 2^{2+}) MS1 isomers have been investigated computationally, in the same conditions that those of the starting $[\text{Ru}^{\text{II}}(\text{NO})]$ (1^{2+} and 2^{2+}) GS isomers. The computed UV-visible spectra are shown in Fig. 7, and the corresponding transitions of interest are shown in Table 4. All of them lead to a significant charge transfer to the iso-nitrosyl (ON) ligand, and hence to a possible back isomerization towards the stable 1^{2+} and 2^{2+} starting isomers.

Something important to point out is that, within the conditions of our experimental setup, the irradiation of the starting $[\text{Ru}^{\text{II}}(\text{NO})]$ species could not be conducted in a continuous range of frequencies. Instead, the set of optical filters available imposed the selection of $\lambda = 473 \text{ nm}$, as the only wavelength compatible with the experimental 440–460 nm range of absorption maxima for the $[\text{Ru}^{\text{II}}(\text{NO})]$ species (Fig. 4). Doing so, the irradiations were performed at slightly lower energies, than those required from the spectra. In order to transpose these experimental conditions to the computational analysis, one has to keep in mind that the theoretical electronic transitions were found to be slightly blue shifted by about 1500 cm^{-1} (30 nm) with respect to the experimental data (Table 3). This leads us to consider the effect of a theoretical irradiation at 441 nm (instead of 473 nm). Doing so, the

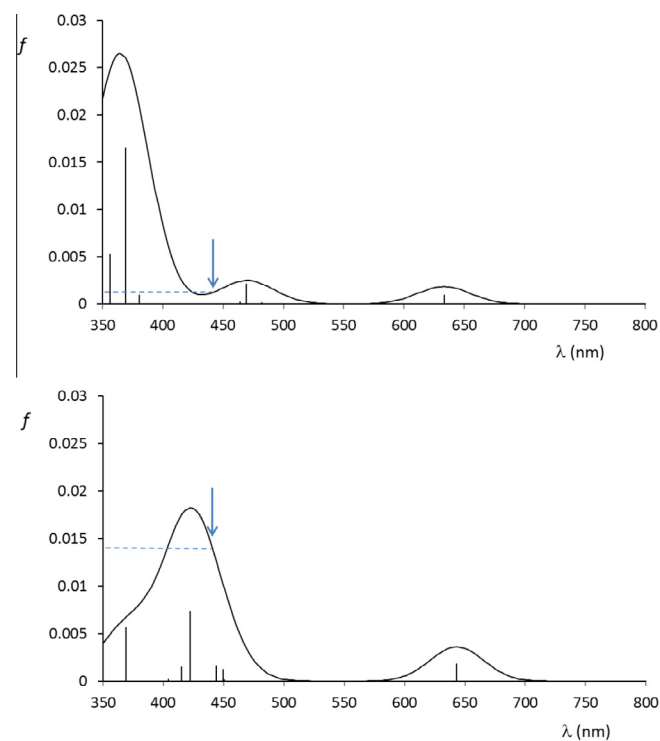


Fig. 7. Computed UV-visible spectra (oscillator strengths f against wavelengths λ) for 1^{2+} (top) and 2^{2+} (bottom). The arrows indicate the wavelength of theoretical irradiation ($\lambda = 441 \text{ nm}$).

Table 4
Comparison of relevant TD-DFT data for 1^{2+} and 2^{2+} : absorption maxima (λ_{max} in nm), oscillator strengths (f), main component and character of the configuration interaction (CI) expansion.

Compound	Transition	λ_{max}	f	Composition of the CI expansion ¹	Dominant character
1^{2+}	1 → 9	469	0.0021	0.346 $\chi_{107 \rightarrow 108}$ + 0.346 $\chi_{106 \rightarrow 109}$ − 0.341 $\chi_{103 \rightarrow 108}$ + 0.321 $\chi_{102 \rightarrow 109}$	$p_{\text{Cl}} + \pi_{(\text{py})} \rightarrow d_{\text{xz}} + d_{\text{yz}} - \pi_{\text{x}}^*(\text{NO}) - \pi_{\text{y}}^*(\text{NO})$
	1 → 18	369	0.0165	0.468 $\chi_{99 \rightarrow 109}$ + 0.468 $\chi_{100 \rightarrow 108}$	$p_{\text{Cl}} + \pi_{(\text{py})} \rightarrow d_{\text{xz}} + d_{\text{yz}} - \pi_{\text{x}}^*(\text{NO}) - \pi_{\text{y}}^*(\text{NO})$
2^{2+}	1 → 9	450	0.0012	0.416 $\chi_{135 \rightarrow 140}$ + 0.416 $\chi_{134 \rightarrow 141}$	$p_{\text{Cl}} + \chi_{(\text{Cl-py})} \rightarrow d_{\text{xz}} + d_{\text{yz}} - \chi_{\text{x}}^*(\text{NO}) - \pi_{\text{y}}^*(\text{NO})$
	1 → 12	444	0.0016	0.419 $\chi_{134 \rightarrow 140}$ + 0.419 $\chi_{135 \rightarrow 141}$	$p_{\text{Cl}} + \pi_{(\text{Cl-py})} \rightarrow d_{\text{xz}} + d_{\text{yz}} - \pi_{\text{x}}^*(\text{NO}) - \chi_{\text{y}}^*(\text{NO})$
	1 → 13	422	0.0073	0.699 $\chi_{133 \rightarrow 140}$	$\pi_{(\text{Cl-py})} \rightarrow d_{\text{yz}} - \pi_{\text{y}}^*(\text{NO})$
	1 → 14	422	0.0073	0.699 $\chi_{133 \rightarrow 141}$	$\pi_{(\text{Cl-py})} \rightarrow d_{\text{xz}} - \pi_{\text{x}}^*(\text{NO})$

Orbitals 133, 135, 140, and 141 are the HOMO − 6, HOMO − 4, LUMO, and LUMO + 1, respectively, for 2^{2+} .

¹ Orbitals 107, 108, and 109 are the HOMO, LUMO, and LUMO + 1, respectively, for 1^{2+} .

experimental conditions can be approached for the 1^{2+} and 2^{2+} ground states and, more importantly, for the 1^{2+} and 2^{2+} metastable states, as well. The effects of such irradiations are shown in Fig. 7 (blue arrows). In the case of 1^{2+} , the irradiation falls in the vicinity of transition 1 → 9, but it corresponds to a weak effective oscillator strength (f) of 0.0012 (top of Fig. 7). By contrast, the irradiation conducted on the metastable 2^{2+} species involves a set of four (1 → 9, 1 → 12, 1 → 13, and 1 → 14) transitions, and leads to an effective f of 0.0140 (bottom of Fig. 7). This higher intensity computed for 2^{2+} suggests a yield of back $\text{Ru}^{\text{II}}(\text{ON}) \rightarrow \text{Ru}^{\text{II}}(\text{NO})$ isomerization much larger in 2^{2+} than in 1^{2+} , in agreement with the experimental data, and the theoretical work previously reported on 1^{2+} [33].

Finally, a last issue has to be addressed in this computational investigation, regarding the understanding of the origin of such different spectra for the metastable 1^{2+} and 2^{2+} isomers, while the stable 1^{2+} than 2^{2+} species exhibit rather similar spectra (Table 3 and Fig. 5). More precisely, the orbitals of the chlorine atoms present in 2^{2+} appear not to contribute significantly to the main transitions of the starting $[\text{Ru}^{\text{II}}(\text{NO})]$ species, thus leading to charge transfer transition nearly identical, with a tendency for enhanced intensities in 2^{2+} , as the only noticeable difference. By contrast, the UV–visible spectrum of 2^{2+} exhibits two very intense (1 → 13, and 1 → 14) degenerated transitions centered at 422 nm, in which the dominant involved orbitals are shown in Fig. 8. Interestingly, the only occupied orbital involved in these transitions is the #133 (HOMO − 6) in which the contribution of the chlorine atoms is dominant. It is therefore not surprising that these intense transitions do not find their counterpart in 1^{2+} , where no chlorine is present, thus leading to so different UV–visible spectra between both species.

3.5. NO release in $[\text{Ru}^{\text{II}}\text{Cl}(\text{NO})(\text{Cl-py})_4](\text{PF}_6)_2$

Photoactive cations deriving from $[\text{Ru}^{\text{II}}\text{Cl}(\text{NO})(\text{py})_4]^{2+}$ have recently witnessed an increasing interest in relation to their capability for providing solid state photo-switches with high yields. Alternatively, there is an additional photoreaction which leads to the release of the biologically active NO^\bullet radical. Clearly, there is no obvious correlation between the NO^\bullet release, which is basically a molecular process, and the photo-switch, which implies various molecular and solid state parameters. Nevertheless, and although the purpose of the present study is dedicated to $\text{NO}^\bullet/\text{ON}^\bullet$ switches, the issue of achieving a NO^\bullet release with these species arises naturally.

Previous investigations conducted on $[\text{Ru}^{\text{II}}\text{Cl}(\text{NO})(\text{py})_4](\text{PF}_6)_2$ have revealed a very modest quantum yield (# NO^\bullet released/# photons absorbed) of 1.6×10^{-3} , thus prohibiting any use of 1^{2+} as a NO^\bullet donor [37]. Nevertheless, the NO^\bullet release from ruthenium-nitrosyls species has been known for over 40 years, and was summarized by Mascharak [38]. Therefore, it is worth checking the NO^\bullet release capabilities of any new $\text{Ru}(\text{NO})$ complexes. In these

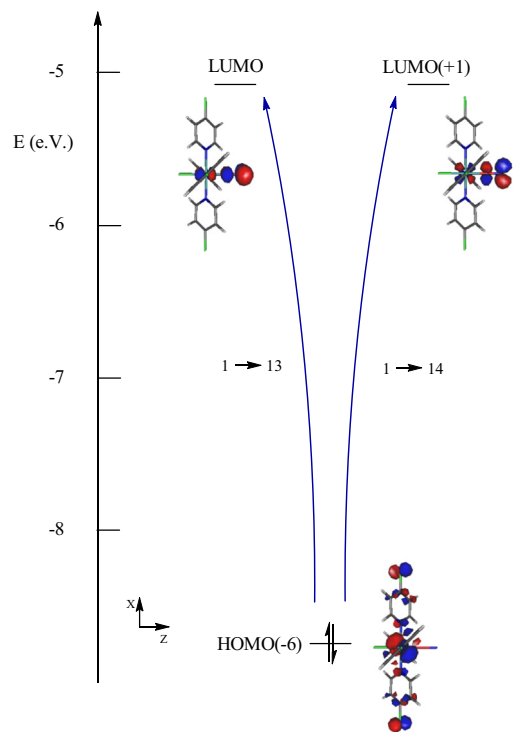


Fig. 8. Dominant orbitals involved in the intense 1 → 13 and 1 → 14 degenerated transitions of 2^{2+} .

experiments, the rapid photo-release is followed by the formation of a solvent bound ruthenium(III) photoproduct, according to the following equation:



This reaction can be followed spectroscopically either by (i) the appearance of a broad and low-lying electronic transition ascribable to a ligand → $\text{Ru}^{\text{III}}(\text{solvent})$ charge transfer, largely red shifted with respect to the related ligand → $\text{Ru}^{\text{II}}(\text{NO})$ charge transfer, or (ii) the appearance of a specific transition involving the use of a NO^\bullet -sensitive sensor. Alternatively, the appearance of a paramagnetic Ru^{III} ion, instead of the close-shell (d^6) Ru^{II} ion, can be checked magnetically.

The changes in the electronic absorption spectra of $[\text{Ru}^{\text{II}}\text{Cl}(\text{NO})(\text{Cl-py})_4](\text{PF}_6)_2$ exposed to 436 nm light in acetonitrile are shown in Fig. S2. The presence of isosbestic points at 314, 450, and 484 nm indicates a clean conversion of the $\text{Ru}^{\text{II}}(\text{NO})$ complexes to related photolyzed species. It is important to note that no back-reaction is observed when the light is turned off. The quantum yield observed for NO^\bullet release at 436 nm light irradiation is 0.29. To confirm that the photoreaction corresponds to the release of nitric

oxide (Eq. (3)), the Griess test has been applied, in which an *in situ* oxidation of the released NO[•] to NO₂⁻ takes place in aqueous medium, under aerobic condition, followed by a reaction with sulfanilamide and naphthylethylenediamine dihydrochloride, thus providing a diazonium cation, and finally the formation of a pink azo dye ($\lambda_{\text{max}} = 540 \text{ nm}$ in CH₃CN/H₂O) [39,40]. The changes observed in the optical spectrum of [Ru^{II}Cl(NO)(Cl-py)₄](PF₆)₂ irradiated at 436 nm in the presence of the Griess reagent are shown in Fig. S3. The gradual appearance of a pink color is clearly evidenced from the experimental data, and undoubtedly proves that NO release takes place under irradiation. It is important to point out that, without irradiation, no color change is evidenced, which indicates the chemical stability of the Ru^{II}(NO) complex.

Importantly, this quantum yield of 0.29 is in the range of quite high NO quantum yields values for ruthenium nitrosyl complexes and indeed much higher than the value of 1.6×10^{-3} , reported on the parent compound [Ru^{II}Cl(NO)(py)₄](PF₆)₂ [37]. However, our attempts to confirm this low value were unsuccessful, the low extinction coefficient ($\epsilon = 151 \text{ mol}^{-1} \text{ L cm}^{-1}$), leading to an insufficient photo-release process, and hence to unreliable experimental data. This limitation must be pointed out to emphasize the fact that any practical biological applications of such ruthenium-polypyridinic species would imply higher extinction coefficients ($\epsilon > 10^3 \text{ mol}^{-1} \text{ L cm}^{-1}$), and lead to the examination of more sophisticated pyridine-based ligands. Nevertheless, although the importance of our result should not be overestimated, as the stability of pyridine and chloride based complexes is far from being insured in biological medium, it confirms that the present species could also be regarded as promising NO sources [34].

4. Conclusion

[Ru^{II}Cl(NO)(py)₄](PF₆)₂ and [Ru^{II}Cl(NO)(Cl-py)₄](PF₆)₂ are two related photo-reactive compounds, however with surprisingly different optical features. While the starting **1**²⁺ and **2**²⁺ ruthenium-nitrosyl cations exhibit nearly similar electronic spectra, leading to a first expectation of similar intrinsic NO/ON switching capabilities, significant differences are predicted in their related **1**²⁺ and **2**²⁺ *iso*-nitrosyl photoisomers, by DFT. In the case of the chloropyridine-based species (**2**²⁺), a significant overlap is found between the UV-spectra of both Ru^{II}(NO) and Ru^{II}(ON) isomers, which prohibits the photo-isomerization from being conducted until completion, by contrast to [Ru^{II}Cl(NO)(py)₄](PF₆)₂ in which the Ru^{II}(NO) → Ru^{II}(ON) and Ru^{II}(ON) → Ru^{II}(NO) transitions are fairly well separated in energy. Alternatively, a surprisingly fast and efficient capability for NO[•] release has been found in [Ru^{II}Cl(NO)(Cl-py)₄](PF₆)₂, with could attract more interest in the future.

Acknowledgements

The authors thank B. Cormary for fruitful discussions. Hasan Shamran Mohammed thanks the Iraqi/French Institution for a Grant, and Campus France – (France) (Moyen-Orient, 776290J) for financial support.

Appendix A. Supplementary data

CCDC 1484591 contains the supplementary crystallographic data for [Ru^{II}Cl(NO)(Cl-py)₄](PF₆)₂. These data can be obtained free of charge via <http://www.ccdc.cam.ac.uk/conts/retrieving.html>, or from the Cambridge Crystallographic Data Centre, 12 Union Road, Cambridge CB2 1EZ, UK; fax: (+44) 1223-336-033; or e-mail: deposit@ccdc.cam.ac.uk. Supplementary data associated with this

article can be found, in the online version, at <http://dx.doi.org/10.1016/j.poly.2016.09.010>.

References

- [1] Photochromism: Memories and Switches, special issue of Chem. Rev. 2000, 100(5). Photochromism: Molecules and Systems, H. Dürr, H. Bouas-Laurent eds. Elsevier, 2003.
- [2] B.L. Feringa (Ed.), Molecular Switches, Wiley-VCH Verlag, 2001.
- [3] V. Balzani, A. Credi, M. Venturi, Molecular Devices and Machines: Concepts and Perspectives for the Nanoworld, second ed., Wiley-VCH Verlag, 2008, Copyright © 2008.
- [4] M. Irie, T. Fukaminato, K. Matsuda, S. Kobatake, Chem. Rev. 114 (2014) 12174.
- [5] G. Berkovic, V. Krongauz, V. Weiss, Chem. Rev. 100 (2000) 1741.
- [6] H.M.D. Bandara, S.C. Burdette, Chem. Soc. Rev. 41 (2012) 1809.
- [7] P. Günter, J.P. Huignard, Photorefractive Materials and their Application, Springer, Berlin, 1988.
- [8] J. Ashley, M.P. Bernal, G.W. Burr, H. Coufal, H. Guenther, J.A. Hoffnagle, C.M. Jefferson, B. Marcus, R.M. Macfarlane, R.M. Shelby, G.T. Sincerbox, IBM J. Res. Develop. 44 (2000) 341.
- [9] S. Kawata, Y. Kawata, Chem. Rev. 100 (2000) 1777.
- [10] N. Tamai, H. Miyasaka, Chem. Rev. 100 (2000) 1876.
- [11] S. Bénard, Y. Pei, Adv. Mater. 12 (2000) 48.
- [12] J. Harada, Y. Kawazoe, K. Ogawa, Chem. Commun. 46 (2010) 2593.
- [13] For a review on solid state switches in N-salicylidene derivatives, see: E. Hadjoudis, I. Mavridis Chem. Soc. Rev. 33 (2004) 579.
- [14] (a) For representative reports on solid state switch in N-salicylidene derivatives, see: D.A. Safin, M. Bolte, Y. Garcia Cryst. Eng. Comm. 16 (2014) 8786; (b) M. Avadanei, V. Cozan, S. Shova, J.A. Paixao, Chem. Phys. 444 (2014) 43; (c) M. Sliwa, S. Létard, I. Malfant, M. Nierlich, P.G. Lacroix, T. Asahi, H. Masuhara, P. Yu, K. Nakatani, Chem. Mater. 17 (2005) 4727.
- [15] (a) A. Patra, R. Métivier, J. Piard, K. Nakatani, Chem. Commun. 46 (2010) 6385; (b) M. Sliwa, S. Létard, I. Malfant, M. Nierlich, P.G. Lacroix, T. Asahi, H. Masuhara, P. Yu, K. Nakatani, Chem. Mater. 17 (2005) 4727.
- [16] (a) U. Hauser, V. Oestrich, H.D. Rohrweck, Z. Physik A 280 (1977) 17–25; (b) U. Hauser, V. Oestrich, H.D. Rohrweck, Z. Physik A 280 (1977) 125.
- [17] (a) T. Woike, H. Zöllner, W. Krasser, S. Haussühl, Solid State Commun. 73 (1990) 149; (b) T. Woike, S. Haussühl, Solid State Commun. 86 (1993) 333; (c) D. Schaniel, T. Woike, C. Boskovic, H.U. Gudel, Chem. Phys. Lett. 390 (2004) 347; (d) D. Schaniel, T. Woike, D. Biner, K. Kraemer, H.U. Gudel, Phys. Chem. Chem. Phys. 9 (2007) 5149; (e) D. Schaniel, T. Woike, N.R. Behrnd, J. Hauser, K. Kraemer, T. Todorova, B. Delley, Inorg. Chem. 48 (2009) 11399.
- [18] J.A. Guida, O.E. Piro, P.J. Aymonino, Inorg. Chem. 43 (1995) 4113.
- [19] D.V. Fomitchev, P. Coppens, T. Li, K.A. Bagley, L. Chen, G.B. Richter-Addo, Chem. Commun. 19 (1999) 2013.
- [20] S.C. Da Silva, D.W. Franco, Spectrochim. Acta, Part A 55A (1999) 1515.
- [21] T.E. Bitterwolf, Inorg. Chem. Commun. 11 (2008) 772.
- [22] (a) B. Cormary, I. Malfant, M. Buron-Le Cointe, L. Toupet, B. Delley, D. Schaniel, N. Mockus, T. Woike, K. Fejfarova, V. Petricek, M. Dusek, Acta Crystallogr. Sect. B 65 (2009) 612; (b) D. Schaniel, B. Cormary, I. Malfant, L. Valade, T. Woike, B. Delley, K.W. Kraemer, H.U. Gudel, Phys. Chem. Chem. Phys. 9 (2007) 3717.
- [23] B. Cormary, S. Ladeira, K. Jacob, P.G. Lacroix, T. Woike, D. Schaniel, I. Malfant, Inorg. Chem. 51 (2012) 7492.
- [24] G. Scalmani, M.J. Frisch, B. Mennucci, J. Tomasi, R. Cammi, V. Barone, J. Chem. Phys. 124 (094107) (2006) 1.
- [25] G.M. Sheldrick, Acta Cryst. A 64 (2008) 112.
- [26] P.V.D. Sluis, A.L. Spek, Acta Crystallogr. Sect. A 46 (1990) 194–201.
- [27] M.J. Frisch, G.W. Trucks, H.B. Schlegel, G.E. Scuseria, M.A. Robb, J.R. Cheeseman, G. Scalmani, V. Barone, B. Mennucci, G.A. Petersson, H. Nakatsuji, M. Caricato, X. Li, H.P. Hratchian, A.F. Izmaylov, J. Bloino, G. Zheng, J.L. Sonnenberg, M. Hada, M. Ehara, K. Toyota, R. Fukuda, J. Hasegawa, M. Ishida, T. Nakajima, Y. Honda, O. Kitao, H. Nakai, T. Vreven, J.A. Montgomery Jr., J.E. Peralta, F. Ogliaro, M. Bearpark, J.J. Heyd, E. Brothers, K.N. Kudin, V.N. Staroverov, R. Kobayashi, J. Normand, K. Raghavachari, A. Rendell, J.C. Burant, S.S. Iyengar, J. Tomasi, M. Cossi, N. Rega, J.M. Millam, M. Klene, J.E. Knox, J.B. Cross, V. Bakken, C. Adamo, J. Jaramillo, R. Gomperts, R.E. Stratmann, O. Yazyev, A.J. Austin, R. Cammi, C. Pomelli, J.W. Ochterski, R.L. Martin, K. Morokuma, V.G. Zakrzewski, G.A. Voth, P. Salvador, J.J. Dannenberg, S. Dapprich, A.D. Daniels, Ö. Farkas, J.B. Foresman, J.V. Ortiz, J. Cioslowski, D.J. Fox, Gaussian 09, Revision E.01, Gaussian, Inc., Wallingford, CT, 2009.
- [28] A.D. Becke, J. Chem. Phys. 98 (1993) 564.
- [29] C. Lee, W. Yang, R.G. Parr, Phys. Rev. B 37 (1988) 785.
- [30] P.J. Hay, W.R. Wadt, J. Chem. Phys. 82 (1985) 270.
- [31] A.W. Ehlers, M. Böhme, S. Dapprich, A. Gobbi, A. Höllwarth, V. Jonas, K.L. Köhler, R. Stegmann, A. Vedkamp, G. Frenking, Chem. Phys. Lett. 208 (1993) 111.
- [32] J. Tomasi, B. Mennucci, R. Cammi, Chem. Rev. 105 (2005) 2999.
- [33] J.S. García, F. Alary, M. Boggio-Pasqua, I.M. Dixon, I. Malfant, J.L. Heully, Inorg. Chem. 54 (2015) 8310.

- [34] J. Akl, I. Sasaki, P.G. Lacroix, I. Malfant, S. Mallet-Ladeira, P. Vicendo, N. Farfán, R. Santillan, Dalton Trans. 45 (2014) 12721.
- [35] G.K. Lahiri, W. Kaim, Dalton Trans. 39 (2010) 4471.
- [36] Th. Woike, W. Krasser, H. Zöllner, W. Kirchner, S. Haussühl, Z. Phys. D 25 (1993) 351–356.
- [37] A.G. De Candia, J.P. Marcolongo, R. Etchenique, L.D. Slep, Inorg. Chem. 49 (2010) 6925.
- [38] N.L. Fry, P.K. Mascharak, Acc. Chem. Res. 44 (2011) 289.
- [39] J.P. Griess, Ber. Deutsch Chem. Ges. 12 (1879) 426.
- [40] D. Tsikas, J. Chromatogr. B 851 (2007) 51.